Optimized Design of a Novel Modular Tubular Transverse Flux Reluctance Machine

Dan-Cristian Popa[1], Dan D. Micu[2], Olivia-Ramona Miron[2], and Loránd Szabó[1]

[1]Department of Electrical Machines and Drives, Technical University of Cluj-Napoca, Cluj-Napoca 400027, Romania
[2]Department of Electrical Engineering, Numerical Methods Research Center, Technical University of Cluj-Napoca, Cluj-Napoca 400027, Romania

This paper presents a new type of tubular electrical machine with a modular construction. The structure of the machine, concerning its construction, is discussed in the first part of the paper. A semi-analytical method based on the magnetic equivalent circuit calculation is used in order to obtain the flux densities in different parts of the iron core of the machine. A Gauss elimination procedure is applied to the system of linear equations resulted from the magnetic equivalent circuit, in order to express the flux in the air gap. The problem of optimization of the traction force is analyzed. The maximization of the function is handled with the Nonlinear Conjugate Gradient method and verified with a Gauss Newton algorithm. An application of the presented theory shows the usefulness of this approach. The results provided by the optimization method applied on a designed tubular machine illustrate its advantages. A numerical analysis performed on both a designed and then optimized structure confirmed the results obtained in the optimization process.

Index Terms—**Electromagnetic force, gradient method, magnetic circuit, numerical analysis, tubular linear machine.**

I. Introduction

THE demand for linear servo-controlled high-speed actuation, with high precision and a high bandwidth, has increased considerably in the past years [1]. One of the main advantages of the linear electromagnetic machines over their rotary-to-linear counterparts is the absence of mechanical gears and transmission systems, which offers higher performance and improved reliability [1]. Hence, electrical machines with linear movement have become more important in common applications such as healthcare [2], [3], transportation [4], [5], and various electrical drives [6].

Linear structures present two topologies: flat-type or tubular. The most important shortcoming of the linear machines with a single-sided flat-type structure is the existence of a significant thrust force between the two armatures [7]. This disadvantage is avoided due to the radial symmetry of the tubular machines or the double-sided flat-type structures which determines the compensation of all the thrust forces acting around the circumference of the air gap. The double sided structures require sophisticated double linear guidance systems, which have to precisely assure the two constant air gaps and also to guide laterally the moving armature together with the stators. On the other hand tubular linear motors need only much simpler linear ball or sleeve bearings. Extended researches have been conducted on flat-type or tubular linear structures with permanent magnets (PM) [8]–[10]. Despite their very good performances (high power and force densities, servo characteristics, efficiency) the drawbacks of such machines, such as the complex manufacturing and high costs must also be considered [7]. Hence, different types of linear machines without permanent magnets (especially those with variable reluctance) can be seen as alternative solutions for different applications. In a former study on tubular linear reluctance motors, several advantages of tubular variable reluctance machines have been demonstrated [9]. An interesting application of such a machine driving a pump for the circulatory heart assistance is reported in [2].

In this paper, a tubular machine with a modular construction is proposed. The machine under study originated from the linear transverse flux reluctance machine with a modular construction. In [12] a flat-type linear transverse flux motor with PM was presented. A simpler structure, without PM, but with similar performances, was analyzed in [13]. In [14] the general structure of the tubular linear transverse flux reluctance machine has been studied. An extended numerical analysis of the tubular motor mentioned above was given in [15]. A comparison between the flat type and tubular transverse flux reluctance machines, showing their fault tolerant capacity and the similarities of the two structures, was presented in [16]. In [17], the technologies used for the construction of this tubular motor and the basic concepts concerning the control of the motor were presented. A prototype of the tubular machine was analyzed and experimental tests were performed in [18]. This paper is focused on the development of an optimized design of the studied tubular machine. The optimization process is based on the maximization of the traction force under the assumption that the volume of the machine remains unchanged.

The modular tubular transverse flux reluctance machine (MTTFRM) operates on the variable reluctance principle and belongs to the transverse flux machine class. The machine is without PM, only with electromagnetic excitation on the stator and passive mover. Its modular construction is presented in the following sections. A particular feature of both the stator and the mover of the machine is the use of magnetic pieces alternating with non-magnetic spacers.

A semi-analytical analysis, based on the magnetic equivalent circuit, is the foundation of the optimization procedure applied for this machine. The force is computed similarly as is in the case of other devices operating on the variable reluctance principle [7]. The optimization procedure is performed in order to obtain the maximum traction force. An optimal solution of the objective function can be found using the direction of its gradient. In order to distinguish between the minimum or the maximum of a function, the matrix of second derivatives has to

Manuscript received November 11, 2012; revised January 25, 2013 and April 19, 2013; accepted June 04, 2013. Date of publication June 18, 2013; date of current version October 21, 2013. Corresponding author: D.-C. Popa (e-mail: Dan.Cristian.Popa@emd.utcluj.ro).

Color versions of one or more of the figures in this paper are available online at http://ieeexplore.ieee.org.

Digital Object Identifier 10.1109/TMAG.2013.2269537

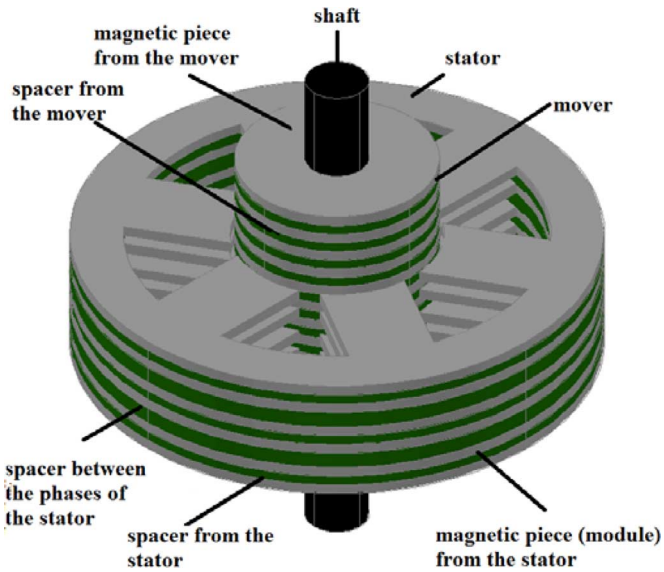

Fig. 1. The structure of the iron core of the proposed MTTFRM.

be investigated. Newton methods, as well as gradient methods are the classical approach when dealing with this type of problems. Features like search directions and global convergence are two main aspects of the optimization [19]. Conjugate gradient methods include a large number of optimization algorithms with strong local and global convergence properties [20], [21]. Two geometric parameters of the machine that influence in different ways the values of the force are considered as variables. The algorithm is applied in order to maximize the force developed in the machine when the exterior dimensions, the length and the exterior diameter, are kept constant.

The results of the numerical analysis performed on a designed and optimized variant are in good agreement with the values obtained from the optimization procedure.

II. Transverse Flux Variable Reluctance Machine

Despite being an old idea, the transverse flux topology was used again at the beginning of the 1980's. Most of the studies focused on the rotary transverse flux machines as the attention paid to the linear variants was much smaller [22].

A. Structure of the Machine

A tubular transverse flux reluctance machine with a modular construction has been studied here. The iron core of the machine is presented in Fig. 1 [14].

In order to have a continuous movement, the minimum number of required N stator phases is three [15]. A phase of the stator of the MTTFRM consists of m magnetic pieces, defined as modules or teeth on the axial direction of movement, separated by non-magnetic pieces, named spacers, Fig. 2. Each module of the stator has the Z poles and slots similar to the structure of the classic SRM stator, Fig. 3(a) [23]. The mover is passive, and consists of simple cylindrical magnetic pieces, forming the teeth of the mover, alternating with non-magnetic spacers. The magnetic pieces of both the stator and the mover can be made either from laminations or from soft magnetic composites (SMC).

The sum of the axial length of a tooth (t_s on the stator, t_m on the mover) and of a spacer (s_s on the stator and s_m on the mover) is the tooth pitch τ, Fig. 2. The pole pitch of the stator and mover

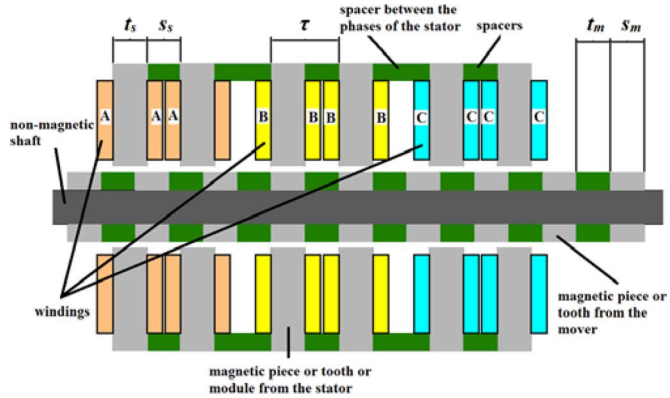

Fig. 2. Longitudinal cross-section view of the proposed MTTFRM.

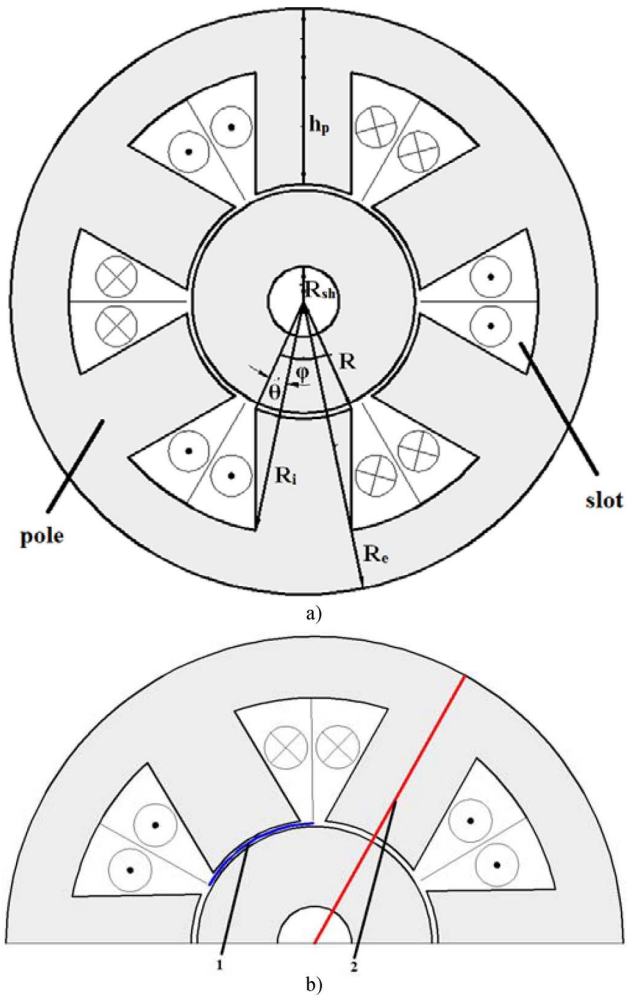

Fig. 3. (a) Transversal section view of the proposed MTTFRM; (b) detail of half of the magnetic piece: (1)—circumferential line in the air gap, (2)—line in radial direction.

must be the same. Furthermore, in [24] it was demonstrated that for such variable reluctance linear machines the maximum force is obtained when the axial lengths of the tooth of the stator and mover are the same $t_s = t_m$. Hence, in all future considerations we will take into account this hypothesis.

In order to work properly as a motor, the modules of the stator phases have to be shifted by $s_m + \tau/N$. This shifting is secured by non-magnetic spacers like the ones used between the stator modules, but with adequate axial length, Fig. 2. The step size of

the motor is given by the ratio of the tooth pitch and the number of phases.

The windings from the stator are obtained by connecting the coils of the module of the stator either in series or parallel. The parallel connection has the advantage because one is obtaining a fault tolerant structure. Concentrated coils around each pole of the module are used for the construction of a module winding, Fig. 3(a) [14].

When energizing a phase of the modules unaligned with the corresponding mover magnetic pieces, Fig. 2—phases A or C, these tend to align with the stator modules. Thus, only the windings of a single phase have the power supplied during a period, meaning that only the modules of this phase generate traction force [14]. The total force is proportional to the number of modules of a phase and the number of poles of a module. From these reasons the design procedure is focused on obtaining the geometric and electric dimensions of a single module for an imposed traction force [25].

The advantages of this topology, in comparison with similar tubular structures, with or without PM, are:

a) the modular structure gives the possibility of an easy assembly of the component parts and allows to increase the force by adding supplementary modules, limited by the imposed length of the machine.
b) simpler structure of the machine and the low cost of its production;
c) the use of spacers that allows reducing the mass;

One of the main shortcomings of the MTTFRM is, like in the case of other transverse flux machines, the high value of the leakage fluxes.

B. Analytical Analysis

The analytical computation has taken into account that the developed force for any linear variable reluctance machine is given by the variation of the magnetic energy in the air gap versus the linear displacement, as expressed in (1) [25]. Considering the air-gap magnetic energy as in (2) and the air-gap volume V on the circumference for a phase, as in (3), the force can be defined as (4):

$$f = \frac{\partial W_m}{\partial x} = \frac{W_f - W_i}{(t_s - x_f) - (t_s - x_i)} \tag{1}$$

$$W = \frac{B_g^2}{2 \cdot \mu_0} \cdot V \tag{2}$$

$$V = m \cdot z \cdot R \cdot \varphi \cdot g \cdot (t_s - x) \tag{3}$$

$$f = \frac{m \cdot z \cdot R \cdot \varphi \cdot g}{2 \cdot \mu_0 \cdot (x_i - x_f)} \cdot \left[B_{gf}^2 \cdot (t_s - x_f) - B_{gi}^2 \cdot (t_s - x_i)\right] \tag{4}$$

where R is the interior radius in the air gap, φ is the stator pole angle, g is the air-gap length, R_{sh} is the shaft radius, as in Fig. 3(a), W_f, W_i, represent the magnetic energy stored in the air gap for the final and the initial conditions respectively; x_f, x_i is the final, respectively the initial axial coordinate, B_{gf}, B_{gi} are the values of the air-gap magnetic flux density in two consecutive positions and μ_0 is the magnetic permeability in the air gap. This equation gives accurate results only for small differences between x_f and x_i.

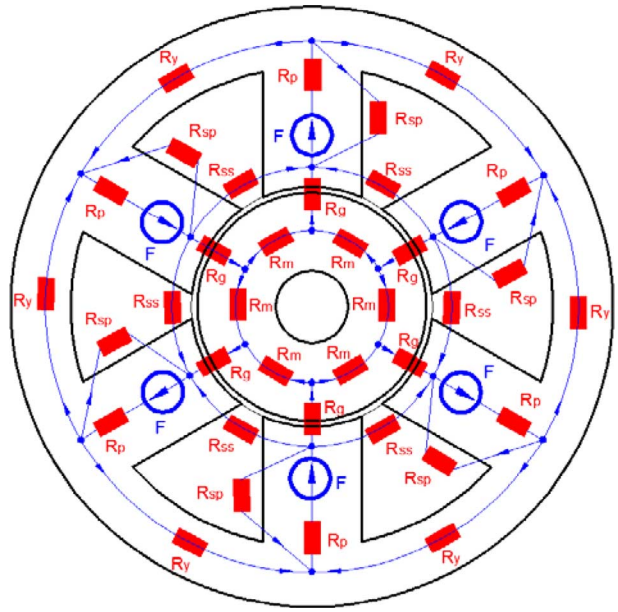

Fig. 4. The reluctance network of a module and the corresponding magnetic part from the mover of the MTTFRM.

The magneto-motive force (mmf) F is a function of the air gap and the flux density in the air gap [23].

$$F = \frac{k_s}{\mu_0} \cdot g \cdot B_{g0} \tag{5}$$

where B_{g0} is the value of the air-gap magnetic flux density in the aligned position having the value imposed at the start of the design procedure, and k_s is the saturation factor [25]. Details about this algorithm can be found in [15].

The results of the design algorithms were verified first semi-analytically by using the magnetic equivalent circuit (MEC) of a module of MTTFRM and the corresponding mover magnetic piece [26]. The first step in obtaining the magnetic equivalent circuit is to create the reluctance network corresponding to the flux tubes flowing in directions perpendicular to the machine axis, Fig. 4. This is based on the plausible assumption that almost all the fluxes flow in radial direction because the axial teeth of both the stator and the mover are separated by non-magnetic pieces. The only flux in axial direction is given by a part of the leakage fluxes around the coils.

The value of F is obtained in the design process with (5). The reluctances: of the yoke R_{my}, pole R_{mp}, air-gap R_{mg} and mover R_{mm} are computed (6) using the geometric dimensions (stator inner and outer radius, stator pole height, stator pole angle, axial length of a tooth, shaft radius, air gap) that resulted from the design procedure and the relative magnetic permeability of the iron core material. The leakage reluctances R_{msp} and R_{mss} are defined considering the paths in the air of the leakage fluxes round the coils and between two neighboring poles, respectively [23]. All the geometric dimensions are represented in Figs. 2 and 3. The dimensions that were used are related to some other geometric dimensions such as: c_{c2}—the insulation between the coil and the iron core, c_{12}—distance between two neighbored coils, a_b—the medium thickness of a coil, k_R—the Rogowski coefficient. The most difficult task is to express the reluctances of the mover and the leakages,

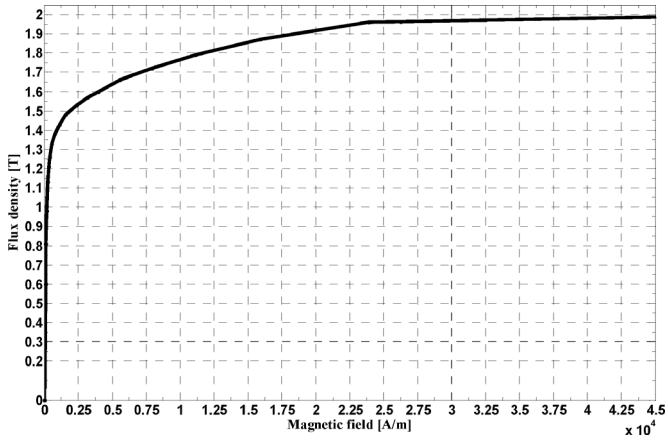

Fig. 5. Magnetization curve of the material used for the construction of the magnetic pieces.

mainly due to the necessity of making some approximations of the length of the flux paths and the active magnetic surface.

$$\begin{cases} R_{mg}=\dfrac{g}{\mu_0\cdot(R-g/2)\cdot\alpha\cdot(t_s+g-x)} \\ R_{mp}=\dfrac{h_p}{\mu_0\cdot\mu_{rp}\cdot R\cdot\varphi\cdot t_s} \\ R_{my}=\dfrac{[(R_t+R_e)/Z]\cdot(\pi+\theta-\varphi)}{\mu_0\cdot\mu_{ry}\cdot(R_e-R_i)\cdot t_s} \\ R_{mm}=\dfrac{\pi\cdot(a_b/2+c_{c2}+R\cdot\varphi/4)+a_b+c_{12}-2g}{\mu_0\cdot\mu_{rm}\cdot(R-1.5R_{sh})\cdot t_s} \\ R_{mss}=\dfrac{1}{\mu_0\cdot g\cdot\left(\dfrac{h_p\cdot\cos\left(\dfrac{\varphi}{2}\right)-h_0}{3R\cdot\left(\dfrac{2\pi}{Z}-\varphi\right)}+\dfrac{h_0}{R\cdot\varphi}\right)} \\ R_{msp}=\dfrac{h_p}{7.92\cdot10^{-6}\cdot k_R\cdot2\cdot(t_s+R\cdot\varphi)\cdot(a_b/3+c_{12}/2)} \end{cases} \tag{6}$$

The expression of the reluctance of the air gap depends on the relative position of the two armatures. Hence, by solving the equations of the magnetic equivalent circuit, different values of the fluxes, and consequently of the force, shall be obtained for each displacement step of the mover with respect to the stator.

The values of the relative magnetic permeability in different parts of the magnetic circuit were computed based on the magnetization curve of the magnetic material used for the magnetic pieces of the machine, given in Fig. 5.

Some of the semi-analytical analyses based on MEC take into account the saturation in different parts of the circuit [27]. In this case, based on a simplifying assumption presented below, the flux densities in different parts of the iron core are computed without neglecting the saturation level that arises.

By considering that variable reluctance machines usually have a saturated iron core [28], one can apply this concept to MTTFRM as well. In [14], [15] authors show that the variation of flux density from the center to the exterior of the machine, Fig. 3(c), proves that the poles are highly saturated, while the yoke and the mover are unsaturated. The situation leads to minor changes in different relative positions of the two armatures. Hence, it can be said that the values of the flux densities in different parts of the iron core of the machine are found on linear parts of the magnetization curve of the magnetic material. Therefore the magnetic permeability in the pole, yoke and mover respectively can be considered constant; and hence the corresponding reluctances can be easily computed.

Due to the necessity to take into consideration the influence of each pole on its neighbors, the resulting magnetic equivalent circuit is rather complex, Fig. 6.

In order to compute the flux density values in different parts of the machine, one must solve the system of equations associated with this magnetic equivalent circuit. These equations were obtained by applying the Kirchhoff's laws to the magnetic equivalent circuit.

The variables in the linear system of equations defined above are the fluxes: through the air-gap Φ_g, through the poles Φ_p, through yoke Φ_y, through mover Φ_m and the leakage ones Φ_{ss} and Φ_{sp}.

$$\begin{cases} \Phi_g+2\Phi_{ss}+\Phi_{sp}-\Phi_p=0 \\ \Phi_p-\Phi_{sp}-2\Phi_y=0 \\ \Phi_g-2\Phi_m=0 \\ 2\Phi_pR_{mp}+\Phi_yR_{my}+\Phi_{ss}R_{mss}-2F=0 \\ \Phi_pR_{mp}+\Phi_{sp}R_{msp}-F=0 \\ 2\Phi_gR_{mg}+\Phi_mR_{mm}-\Phi_{ss}R_{mss}=0 \end{cases} \tag{7}$$

The flux density in the air-gap B_g, which is the ratio between the flux through the air-gap Φ_g and the air-gap surface, can be expressed analytically, as a function of the mmf F and of the reluctances in the circuit. Generally, this can be developed as the function of the mmf, geometric dimensions and magnetic permeability in various parts of the machine. The expression for Φ_g was computed from (7) by means of a Gauss elimination technique.

By computing the traction force with (4), where the fluxes in two consecutive positions were obtained from (8), shown at the bottom of the page, resulted in the general expression of the medium value of the force over a certain interval. The precision of the estimated force increases as the considered interval is smaller.

C. Application

The main parameters of a designed MTTFRM are given in Table I. Steel 111 XC was used for the construction of the iron core.

The computed values of the flux densities in different parts of the machine for the aligned position of the armatures using MEC are given in Table II.

The maximum force computed by using (4) is 165.43 N. This value can be maximized, considering the exterior dimensions

$$\Phi_g=\frac{4\cdot F\cdot R_{mss}\cdot R_{msp}}{R_{mss}\cdot(4\cdot R_{mg}+R_{mm})\cdot(R_{mp}+R_{msp})+(4\cdot R_{mg}+R_{mss}+R_{mm})\cdot(4\cdot R_{msp}\cdot R_{mp}+R_{msp}\cdot R_{my}+R_{my}\cdot R_{mp})} \tag{8}$$

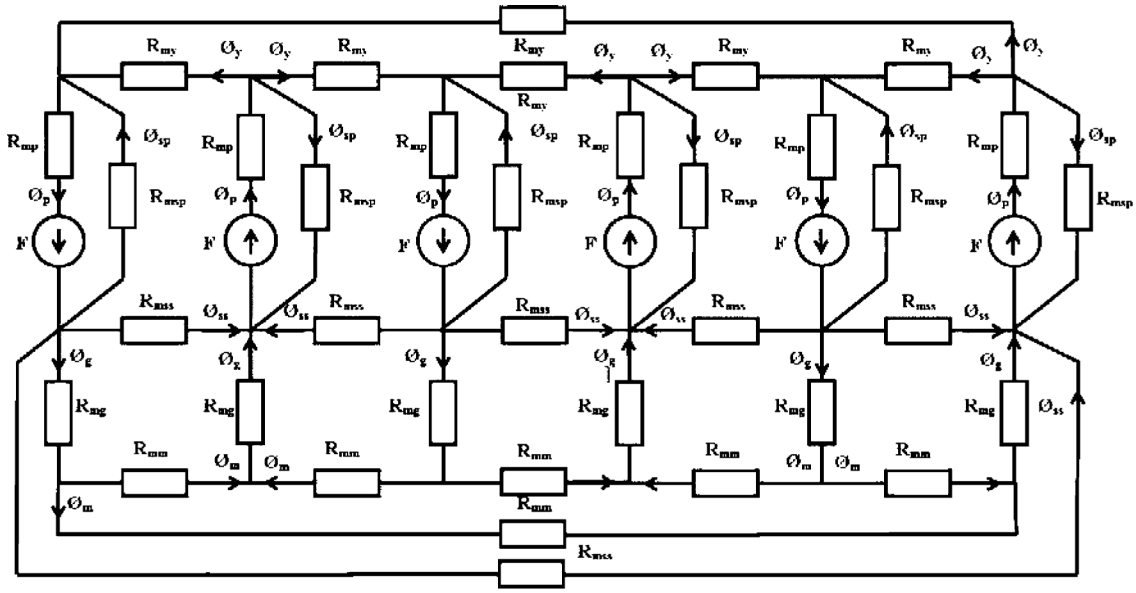

Fig. 6. Magnetic equivalent circuit of a module and the corresponding magnetic part from the mover of the MTTFRM.

TABLE I
IMPOSED AND COMPUTED VALUES AT THE DESIGNED MTTFRM

Nomenclature	Parameter	Type	Value
f_t	Maximum tangential force	Imposed	180 N
N	Number of phases	Imposed	3
m	Number of modules	Imposed	2
z	Number of stator poles	Imposed	6
$t_s = t_m$	Axial length of the stator and mover tooth	Imposed	5 mm
$s_s = s_m$	Axial length of a stator and mover spacer	Imposed	5 mm
τ	Pole pitch	Imposed	10 mm
B_{g0}	Air-gap flux density in aligned position	Imposed	1.3 T
φ	Stator pole angle	Imposed	50^o
g	Air-gap	Imposed	0.5 mm
R	Stator inner radius	Computed	48 mm
h_p	Height of stator poles	Computed	40 mm
R_e	Stator outer radius	Computed	125 mm
R_{sh}	Shaft radius	Computed	10 mm
f'_t	Maximum tangential force	Computed	165.43 N
F	Magneto-motive force	Computed	1280 Aturns
μ_{rp}	Relative permeability of the pole	Imposed	100
$\mu_{ry,}$	Relative permeability of the yoke	Imposed	920
μ_{rm}	Relative permeability of the mover	Imposed	1100
K_{fill}	Fill factor of the slot	Computed	0.2

constant and by applying the optimization procedures that will be described in the next section.

D. Numerical Analysis

The performances of electromagnetic devices can be verified by means of numeric computation (the finite element method FEM). The commercial package Flux 3D is used.

TABLE II
VALUES OF THE FLUX DENSITY IN DIFFERENT PARTS OF THE MTTFRM OBTAINED FROM ANALYTICAL ANALYSIS IN ALIGNED POSITION

Flux density	Machine part	Value
B'_{g0}	Air-gap	1,23 T
B_p	Pole	1.85 T
B_y	Yoke	1.05 T
B_m	Mover	0.87 T

The numerical analysis was focused on the flux density distribution and the force developed in the machine. Although 2D analysis would be much simpler, requiring a less complex model, less time and less computer resources, the structure of the MTTFRM can be modeled only by using a 3D analysis [22]. This is due to the flux paths that are perpendicular to the direction of movement. The software gives the possibility to construct a parameterized geometry of the model. In the numerical analysis, performed in the 'magneto-static' module of Flux 3D, a displacement step of 0.5 mm between the relative positions of the two armatures was considered. These are the same conditions like those considered in the semi-analytical analysis where we have obtained different values of the force for each relative position of the mover with respect to the stator.

Two major issues must be considered when creating the analysis model. As mentioned in previous sections and underlined by formula (4), the force is proportional to the number of modules of a phase and the number of poles of a module. By taking into consideration the radial symmetry of the MTTFRM, the numerical model can be reduced to a single pole of a stator module, the neighboring slots and the corresponding mover part, Fig. 7.

The total force was calculated as being equal to the product between the value obtained in the simulation, the number of poles of a module and the number of modules of a phase. For this machine the multiplying factor is 12.

The mesh of the model, Fig. 8, had 107,464 nodes and 633,783 volume elements. The percentage of excellent quality elements was 63.37%, while the percentage of poor quality

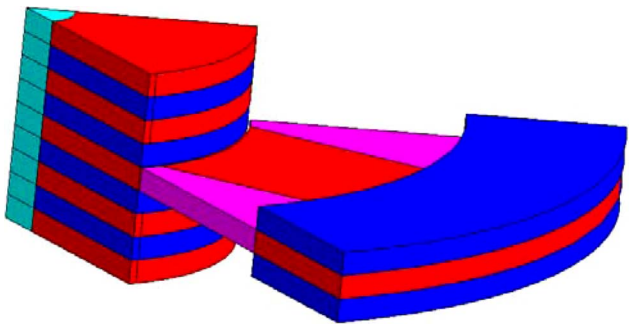

Fig. 7. 3D model of the MTTFRM created for the numerical analysis (the coil wound on the pole is not shown).

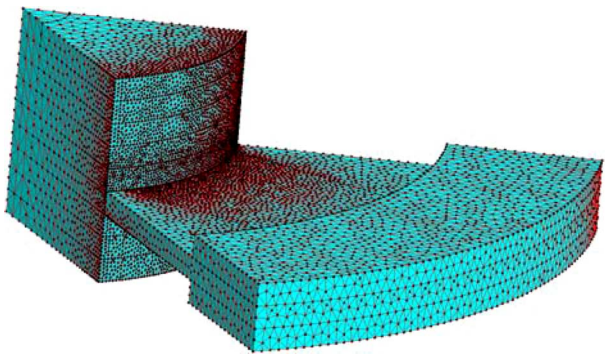

Fig. 8. Mesh of the 3D model of the analyzed MTTFRM.

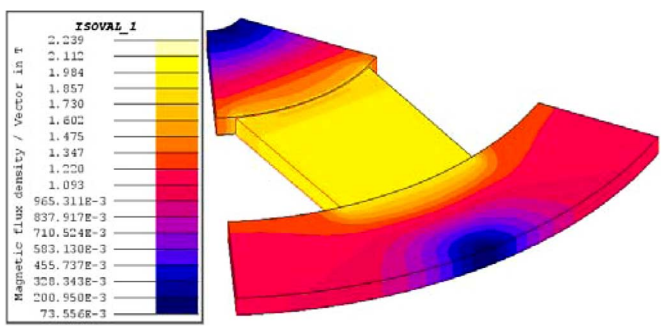

Fig. 9. Flux density map in the pole of a module and the corresponding stator yoke and mover part in the aligned position.

elements was 0.59%. These values assured fairly accurate results.

The flux density map in the structure is presented in Fig. 9. The plots confirm that the pole was saturated, while the yoke and the mover had the flux density values significantly reduced.

The flux density in the air gap evidences a good accordance with the semi-analytical analysis, Fig. 10. The variation was obtained on line (1) presented in Fig. 3(b). The maximum flux density in the aligned position was 1.27 T, which is in close agreement to the imposed value.

The magnetic permeability had small variations in the pole, yoke and mover respectively function of the displacement of the mobile armature with respect to the stator, as mentioned in the previous paragraphs of this section. This statement is supported by variation of the flux density in the radial direction, from the center to the exterior of the machine.

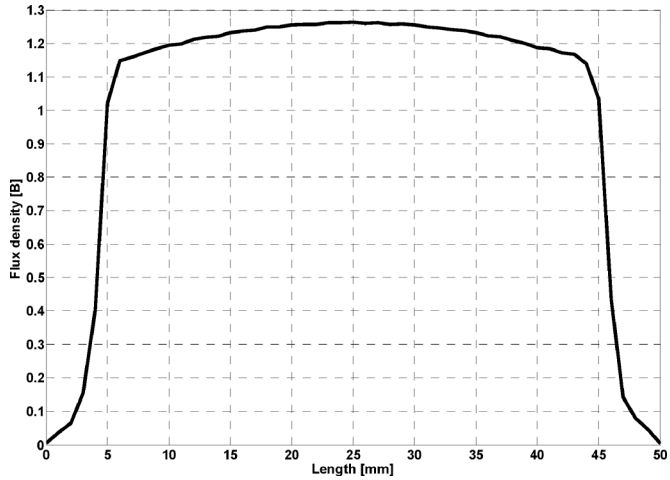

Fig. 10. Air-gap flux density variation in the aligned position.

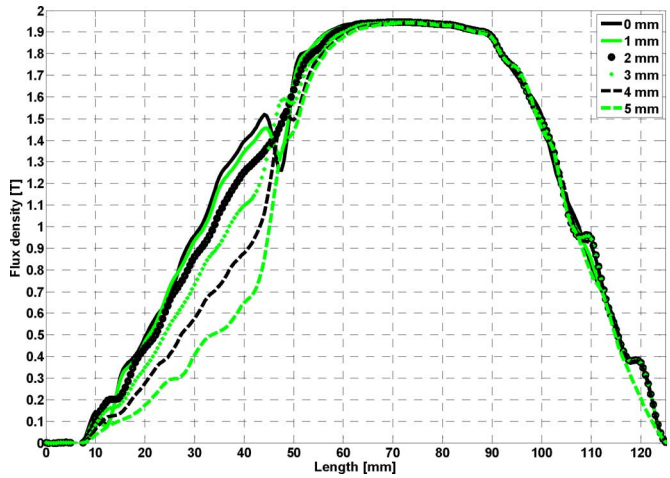

Fig. 11. Flux density distribution in the machine in radial direction (from center to exterior) for different shifting between the two armatures.

The variation of the flux density plotted on line (2) given in Fig. 3(b), for various relative positions of the two armatures, is presented in Fig. 11.

The maximum force obtained for the designed machine was 174.13 N. The difference between this value and the one obtained by the semi-analytical analysis is 6%. The obtained variation of the force shall be presented in the next section in comparison with the one obtained on the optimized structure.

The maximum force density of the designed MTTFRM has been obtained for the intermittent functioning service (S3), at a relative time of operation of 40%. A maximum value of $2.3 \cdot 10^5$ N/m^3 was obtained from the numerical analysis. In [18], the motor operating in the continuous functioning service (S1) was analyzed. The maximum force density resulted from the numerical analysis was $1.48 \cdot 10^5$ N/m^3, while the experimental tests had led to a value of $1.35 \cdot 10^5$ N/m^3. A relatively good agreement between the numerical analysis and experimental results has been found.

These results demonstrate the potential of this low-cost, easy to build machine. From this point of view, the MTTFRM is prefered to the tubular machine with linear interior permanent magnets (TL-IPM), where the force density can be up to $3.4 \cdot 10^5$ N/m^3 or to the tubular linear surface-mounted PM (TL-SPM)

motors where values of $2.2 \cdot 10^5$ N/m^3 have been determined [29].

III. Optimization Problem

The goal of the optimization procedure was to obtain a maximized value for the traction force under the assumption that all the exterior geometric dimensions, as well as the stator inner radius, were kept constant. The traction force is in fact an electromagnetic force. Due to this aspect, in this case, the use of the term electromagnetic force was more appropriate.

The expression of the force evidenced that some of the geometric parameters, like the axial length of a tooth (module), greatly influence its value. The variation of the force for this type of machine on half of the pole pitch is almost sinusoidal [7], [28].

The problem of maximizing the value of the electromagnetic force obtained with (4) was subjected to an optimization procedure. The expression for the force is nonlinear and therefore adequate nonlinear methods were used in order to perform the optimization of the machine with respect to its geometrical dimensions. The force formula (4) was rewritten in terms of the optimization parameters (the axial length of a tooth and the shaft radius) (9).

$$f(t_s, R_{sh}) = \frac{m \cdot z \cdot R \cdot \varphi \cdot g}{2 \cdot \mu_0 \cdot (x_i - x_f)} \cdot \left[\left(\frac{\Phi_{gf}(t_s, R_{sh})}{S_{gf}} \right)^2 \cdot (t_s - x_f) - \left(\frac{\Phi_{gi}(t_s, R_{sh})}{S_{gi}} \right)^2 \cdot (t_s - x_i) \right] \quad (9)$$

The fluxes through the air-gap in two consecutive positions, Φ_{gf} and Φ_{gi}, were computed with (9). S_{gf} and S_{gi} were the active surfaces of the air-gap in the considered positions.

In order to optimize the value of the developed force in a preset interval, certain relative positions of the mover to the stator must be considered. Consequently, we obtained an overdetermined nonlinear system with three equations and one unknown (t_s). The method of nonlinear least squares is the classical approach when dealing with a parameterized application [30].

A nonlinear overdetermined system of equations can be written:

$$F(u) = 0, \quad F: R^m \to R^n \quad (10)$$

where $m > n$. Solving a nonlinear system where multiple solutions exist is complicated and has high computational complexity [31].

The aim was to find the vector u of the unknown parameters such that the function fits best the given data, i.e., the objective function is maximized. This occurs when the gradient of $f(u)$ is equal to zero.

The solution u of the optimal parameters can be found by solving the normal equations:

$$(J^T J)u = J^T r \quad (11)$$

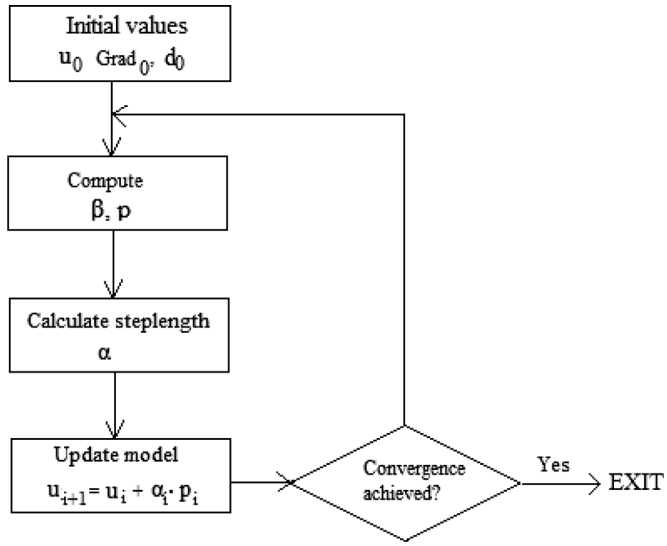

Fig. 12. Flowchart of the optimization process.

where J is the Jacobian matrix, while J^T is the transpose matrix of J and r is the residual vector.

These equations can be solved using various matrix decompositions like the Cholesky decomposition, LU factorization or the Newton methods [32]. The result is obtained iteratively, with values refined by successive approximations:

$$u_j^{k+1} = u_j^k + \Delta u_j, \quad j = 1 \ldots m \quad (12)$$

Because most of those algorithms proceed by minimizing the objective function, the maximization problem proposed in this section, f can easily be adapted by minimizing $-f$. The standard way of solving a nonlinear problem is by the iteration of a linearized problem. In this case, the nonlinearity was handled with two different optimization algorithms: the Newton-Gauss and the Nonlinear Conjugate Gradient method (NCG) [33].

The Nonlinear Conjugate Gradient method is an optimization technique that uses the gradient to find the minimum of a nonlinear function and has low memory requirements [34]. It has been successfully applied for the optimization of fuel consumption in engine industry [35]. A flowchart of the method was conceived in order to present the basic steps, Fig. 12.

Using a sequence of conjugate directions, the optimal location was found by successive approximations:

$$u_{k+1} = u_k + \alpha_k \cdot d_k \quad (14)$$

where u is the vector of the optimization parameters, and the steplength, α, was refined at each iteration by applying an exact line search technique, (α was chosen so that the function $f(u + \alpha \cdot d)$ is minimized). Setting the gradient of the function to zero, the steplength was determined using the Newton-Raphson method:

$$\nabla f(u + \alpha d) = 0 \quad (15)$$

The iterative Newton-Raphson algorithm relies on the Taylor approximation and requires the second derivative of $f(u+\alpha \cdot d)$ with respect to α.

$$\begin{aligned}
&NCG(Grad, Hessian, u_0, N) := \left| \begin{array}{l}
\text{for } i \in 0..N \\
\quad d_{i+2} \leftarrow \text{if}\left(\dfrac{\left|Grad(u_{i+1}) \cdot Grad(u_{i+1})\right|}{\left|Grad(u_0) \cdot Grad(u_0)\right|} \le \varepsilon \text{ , break, } -Grad(u_{i+1}) \right) \\
\quad \beta_{i+1} \leftarrow \dfrac{d_{i+2} \cdot (d_{i+2} - d_{i+1})}{d_{i+1} \cdot d_{i+1}} \\
\quad p_{i+1} \leftarrow d_{i+2} + \beta_{i+1} \cdot p_i \\
\quad \alpha_{i+1} \leftarrow -\dfrac{p_{i+1} \cdot Grad(u_{i+1})}{p_{i+1} \cdot Hessian(u_{i+1}) \cdot p_{i+1}} \\
\quad u_{i+2} \leftarrow u_{i+1} + \alpha_{i+1} \cdot p_{i+1} \\
u
\end{array} \right. \\
&\qquad \text{// starting the iterative calculus} \\
&\qquad \text{// setting the initial direction search as the negative of the gradient} \\
&\qquad \text{// NCG parameter calculated according to Polak-Ribiere formula} \\
&\qquad \text{// update of the search direction} \\
&\qquad \text{// calculating the steplength} \\
&\qquad \text{// iterative process for finding the optimal solution} \\
&\qquad \text{// vector of the succesive approximations of the solution}
\end{aligned}$$

Fig. 13. NCG implemented algorithm.

Setting the first descent direction as the negative of the gradient and computing the first two iterations, the NCG algorithm implemented in Mathcad 14.0 is given in Fig. 13.

With Grad we denoted the gradient of the objective function f and parameter β was computed according to the Polak-Ribiere formula that often converges faster than the Fletcher-Reeves [36]. ε was the error tolerance imposed for the NCG, [37].

The second derivative, encountered in α formula, also known as the Hessian matrix, can be nearly singular in some cases and difficult to invert. In order to improve the conditioning number and speed-up convergence, different methods of preconditioning can be used [38]. Due to the fact that the present NCG algorithm was fast convergent and that the second derivative was non-singular in the preset interval, the preconditioning of the Hessian matrix was not needed [20].

The validation of the results was done with the regularized Newton-Gauss formula as described in [38]. The solution was found by successive approximations of the iterative expression:

$$u_{k+1} = u_k - \left[\left(\gamma \cdot I + J_k^T \cdot J_k\right)\right]^{-1} \cdot \left[J_k^T (f(u_k)_k - y) + \gamma(u_k - u_0)\right] \quad (16)$$

where γ is a regularization parameter greater than zero and I is the identity matrix.

If an extension of the interval needs to be considered then a neural network analysis can be performed, starting from a set of optimized values [39].

IV. Optimization of the Designed MTTFRM

A. Analytical Analysis

In order to obtain the maximum value of the electromagnetic force, the axial length of the tooth t_s is varied keeping the value of the tooth pitch constant. The force is computed for six different relative positions of the mover with respect to the stator. The starting point was with the teeth of a stator phase aligned with the mover ones and the last point is considered to be their misaligned position, Fig. 2, in lateral phases. The interval of the axial length of a tooth is given by the geometrical limitations. Starting from a value of 3.5 mm, t_s can be extended up to 5.5 mm. The shifting between the stator teeth of a phase, misaligned with the mover teeth, was 3.3 mm. In (4), the step of two consecutive magnetic flux density values, chosen to be of the same order of magnitude as the air-gap, was set to 0.5 mm. A smaller value for the step did not induce a significant change for the values of the force. A relative error of $1.019 \cdot 10^{-4}$ resulted. Therefore, the following computations used 0.5 mm for the step between two consecutive forces. The value of t_s obtained with a NCG error tolerance of 10^{-6}, corresponding to the maximum value of the electromagnetic force, was 3.925 mm. Fig. 14 depicts the convergence process of the method.

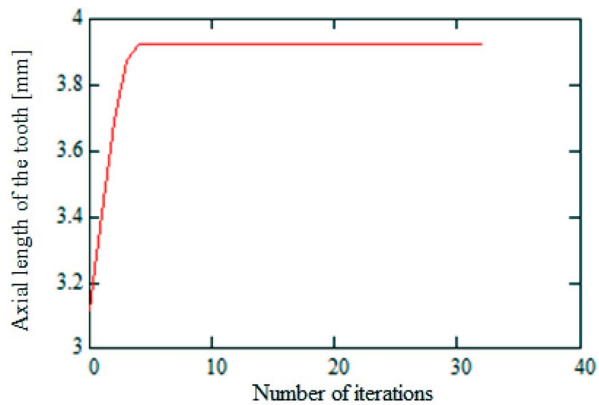

Fig. 14. Convergent process for the optimization algorithm.

It can be noticed that the NCG convergence was achieved in several steps. The optimal solution was been found in 2 m 56 s after eight iterations. The algorithm proved to be convergent even if the initial value was far from the optimum.

The minimization of the objective function with NCG method is presented in Fig. 15.

Therefore, it can be concluded that the solution found with the NCG method on the a priori given interval is a global minimum [32]. The result attained with the Newton-Gauss algorithm yielded to a value of 3.954 mm. For this value the force is 190.35 N, which is an increase of 15% with respect to the force developed for the initial MTTFRM configuration.

When the optimization considered two variables, slightly different results were found. A second analysis with t_s and R_{sh} as the optimization parameters was carried out. The values of R_{sh}

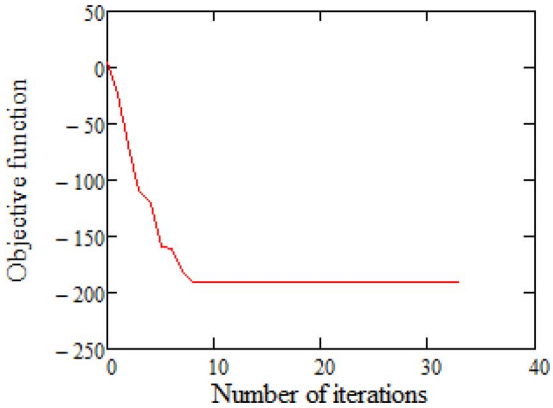

Fig. 15. The minimization of the objective function using NCG method.

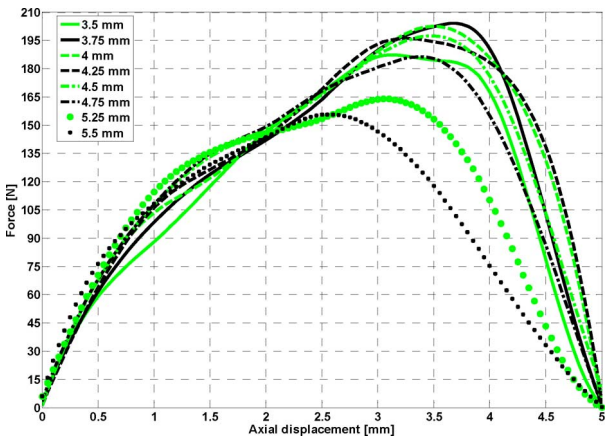

Fig. 16. Force variation on half of the pole pitch for various lengths of the axial tooth obtained from numerical analysis.

were considered to be between 6 and 14 mm. An optimum solution was found when R_{sh} is 11.2 mm. The resulting t_s value was 3.871 mm. The electromagnetic force was 193.91 N. The difference between the optimization with one and two parameters was less than 1%.

B. Numerical Analysis

In the numerical analysis, in order to obtain the maximum value of the developed force an interval between 3.5 and 5.5 mm, with a step of 0.25 mm, was considered for the value of the axial length of a tooth, Fig. 16. The major shortcoming encountered in this analysis was the fact that the optimal value, which corresponds to the maximum force, is usually skipped due to the practical impossibility of taking into account all the values in the considered interval.

A numerical analysis can provide only the interval where the maximum force can be found. The maximum value of the force was obtained for different shifting of the teeth of the two armatures when different values of the axial length of a tooth were considered. When this value was increased due to a smaller shifting between the teeth, a lower force resulted.

The maximum value of the force was obtained for an axial length of the tooth of 3.75 mm and it was 202.2 N. A difference of 15.9% with respect to the initial designed variant resulted. A conclusion of this numerical analysis is that the maximum value of the electromagnetic force can be obtained for a value of t_s between 3.75 mm and 4 mm.

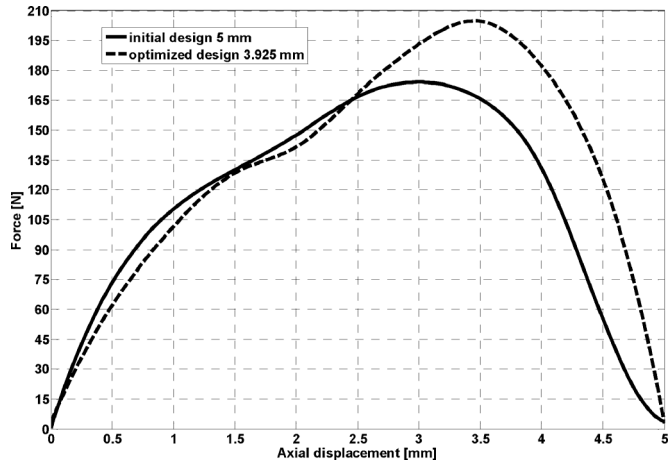

Fig. 17. Force variation on half of the pole pitch for the initial and optimized machine obtained from numerical analysis.

The optimization procedure developed with the NCG algorithm gave a value of 3.925 mm for the axial length of the teeth; this value corresponds to the maximum force [40]. A numerical analysis was carried out in this situation as well. In Fig. 17 a comparison of the forces between the initial and optimized design is presented. The maximum force developed by the optimized MTTFRM was 204.66 N and represents an increase of 17.5% with respect to the value obtained from numerical analysis for the initial variant. A small difference between the force values of the analytical optimization and the numerical analysis resulted. It is very important to underline that the maximum value of the force was obtained in both cases for the same axial length of the tooth.

The value of the axial length of the tooth greatly influenced the developed force. However, the value of the shaft radius affected only the mover reluctance, so its influence on the performance of the machine should be smaller. The numerical analysis considered values between 6 and 14 mm for the shaft radius, with a step of 1 mm. The maximum force of 205.3 N was obtained for a shaft radius of 11 mm and it was slightly larger than for the initial shaft radius. This value was close to that obtained from the optimization procedure.

The maximum force density of the optimized MTTFRM was obtained, as in the case of the initial variant, when the motor would operate in an intermittent functioning service (S3) at a relative time of operation of 40%. The obtained value of $2.7 \cdot 10^5$ N/m^3 confirms the increase of force computed by numerical means.

V. Conclusion

The present paper deals with the optimization of a new type of tubular machine with a modular construction. The basic concepts of the configuration of the design were presented. A semi-analytical analysis based on the magnetic equivalent circuit method was carried out and the results were in a good agreement with the imposed design data. The developed force was expressed as a function of the flux densities obtained from the system of equations associated with the magnetic equivalent circuit. The expression of the force depends on certain geometric parameters and was subjected to an optimization

procedure. The nonlinear conjugate gradient algorithm was used to maximize the electromagnetic force in the MTTFRM.

The machine with the optimized value of the axial length of the tooth was numerically analyzed using Flux 3D. A satisfactory agreement between the numerical analysis and the values obtained with NCG resulted.

An optimized MTTFRM is under construction. Further work is focused on the validation of the numerical optimized results with experimental data.

ACKNOWLEDGMENT

This work was supported by a grant of the Romanian National Authority for Scientific Research, CNDI-UEFISCDI, project number PCCA191/2012.

REFERENCES

[1] J. Wang, G. W. Jewell, and D. Howe, "A general framework for the analysis and design of tubular linear permanent magnet machines," *IEEE Trans. Magn.*, vol. 35, no. 3, pt. 2, pp. 1986–2000, May 1999.

[2] N. Martinez, P. Leprince, and B. Nogarede, "A novel concept of pulsatile magnetoactive pump for medical circulatory support," in *ICEM Elect. Mach.*, 2008, pp. 1–6.

[3] M. Watada, K. Yanashima, Y. Oishi, and D. Ebihara, "Improvement on characteristics of linear oscillatory actuator for artificial hearts," *IEEE Trans. Magn.*, vol. 29, no. 11, pp. 3361–3363, Nov. 1993.

[4] J. Wang, W. Wang, and K. Atallah, "A linear permanent-magnet motor for active vehicle suspension," *IEEE Trans. Veh. Technol.*, vol. 60, no. 1, pp. 55–63, Jan. 2011.

[5] J. Wang, D. Howe, and Z. G. Lin, "Comparative studies on linear motor topologies for reciprocating vapor compressors," in *2007 IEEE Int. Electric Machines Drives Conf.*, 2007, vol. 2, pp. 364–369.

[6] C. Henaux, B. Nogarede, and D. Harribey, "A new concept of modular permanent magnet and soft magnetic compound motor dedicated to widespread application," *IEEE Trans. Magn.*, vol. 48, no. 6, pp. 2035–2043, Jun. 2012.

[7] I. Boldea, *Linear Motion Electromagnetic Devices*. New York, NY, USA: Taylor & Francis, 2001.

[8] H. Chang-Chou, L. Ping-Lun, and L. Cheng-Tsung, "Optimal design of a permanent magnet linear synchronous motor with low cogging force," *IEEE Trans. Magn.*, vol. 48, no. 2, pp. 1039–1042, Feb. 2012.

[9] B. L. J. Gysen, K. J. Meessen, J. J. H. Paulides, and E. A. Lomonova, "3-D analytical and numerical modeling of tubular actuators with skewed permanent magnets," *IEEE Trans. Magn.*, vol. 47, no. 9, pp. 2200–2212, Sep. 2011.

[10] C. Urban, R. Gunther, T. Nagel, R. Richter, and R. Witt, "Development of a bendable permanent-magnet tubular linear motor," *IEEE Trans. Magn.*, vol. 48, no. 8, pp. 2367–2373, Aug. 2012.

[11] B. Tomczuk and M. Sobol, "Field analysis of the magnetic systems for tubular linear reluctance motors," *IEEE Trans. Magn.*, vol. 41, no. 4, pp. 1300–1305, Apr. 2005.

[12] D. C. Popa, L. Szabo, and V. Iancu, "Linear transverse flux motor for conveyors," in *Proc. 6th Int. Symp. Linear Drives for Industrial Application (LDIA)*, Lille, France, 2007, paper no. 188, on CD.

[13] D. C. Popa, L. Szabo, and V. Iancu, "Improved design of a linear transverse flux reluctance motor," in *Proc. 11th Int. Conf. Optimization of Electrical and Electronic Equipment (OPTIM'2008)*, Braşov, Romania, 2008, pp. 136–141.

[14] D. C. Popa, L. Szabo, V. I. Gliga, and V. Iancu, "Design of novel tubular transverse flux reluctance machine," in *Proc. 8th Int. Symp. Linear Drives for Industrial Application (LDIA)*, Eindhoven, Netherlands, 2011, paper no. 183, on CD.

[15] D. C. Popa, V. I. Gliga, L. Szabo, and V. Iancu, "Tubular transverse flux variable reluctance motor in modular construction," in *Proc. 13th Int. Conf. Optimization of Electrical and Electronic Equipment (OPTIM'2012)*, Braşov, Romania, 2012, pp. 572–577.

[16] V. Iancu, D. C. Popa, and L. Szabo, "Fault tolerant modular linear transversal flux reluctance machines," *J. Comput. Sci. Control Syst.*, pp. 1–4, 2009, Romania.

[17] V. I. Gliga, D. C. Popa, and V. Iancu, "Modular transversal flux tubular machine—Presentation and progress achievements," Annals of the University of Craiova, 2011, pp. 1–6, Electrical Engineering series, No. 35, ISSN 1842-4805.

[18] D. C. Popa, V. I. Gliga, and L. Szabo, "Theoretical and experimental study of a modular tubular transverse flux reluctance machine," *Progr. Electromagn. Res.*, vol. 139, pp. 41–55, 2013.

[19] C. Gilbert and J. Nocedal, "Global convergence properties of conjugate gradients methods for optimization," *SIAM. J. Optim.*, vol. 2, no. 1, pp. 21–42, 1992.

[20] W. W. Hager and H. Zhang, "A survey of nonlinear conjugate gradient methods," *Pacific J. Optim.*, no. 2, pp. 35–58, 2006.

[21] Z. Badics and Z. J. Cendes, "A Newton Raphson algorithm with adaptive accuracy control based on a block-preconditioned conjugate gradient method," *IEEE Trans. Magn.*, vol. 41, no. 5, pp. 1652–1655, Sep. 2005.

[22] J. Chang, D. H. Kang, I. A. Viorel, and L. Strete, "Transverse flux reluctance linear motor's analytical model based on finite-element method analysis results," *IEEE Trans. Magn.*, vol. 43, no. 4, pp. 1201–1204, Apr. 2007.

[23] R. Krishnan, *Switched Reluctance Motor Drives—Modeling, Simulation, Analysis, Design, and Applications, Industrial Electronics Series*. Boca Raton, FL, USA: CRC Press, 2001.

[24] P. Acarnely, *Stepping Motors: A Guide to Theory and Practice*. Stevenage, Herts, U.K.: IET, 2002.

[25] I. A. Viorel, K. Hameyer, and L. Strete, "Transverse flux tubular switched reluctance motor," in *Proc. 11th Int. Conf. Optimization of Electrical and Electronic Equipment (OPTIM 2008)*, Braşov, Romania, 2008, pp. 131–136.

[26] J. K. Kim, S. W. Joo, S. C. Hahn, J. P. Hong, D. H. Kang, and D. H. Koo, "Static characteristics of linear BLDC motor using equivalent magnetic circuit and finite element method," *IEEE Trans. Magn.*, vol. 40, no. 2, pp. 742–745, Mar. 2004.

[27] H. Gholizad, B. Funieru, and A. Binder, "Direct modeling of motional eddy currents in highly saturated solid conductors by the magnetic equivalent circuit method," *IEEE Trans. Magn.*, vol. 45, no. 3, pp. 1016–1019, Mar. 2009.

[28] G. Henneberger and I. A. Viorel, *Variable Reluctance Electrical Machines*. Aachen, Germany: Shaker Verlag, 2001.

[29] N. Bianchi, S. Bolognani, D. D. Corte, and F. Tonel, "Tubular linear permanent magnet motors: An overall comparison," *IEEE Trans. Ind. Appl.*, vol. 39, no. 2, Mar./Apr. 2003.

[30] R. V. Dukkipati, *Numerical Methods*. New Delhi, India: New Age International (P) Limited, 2010.

[31] J. Nocedal and S. J. Wright, *Numerical Optimization*. New-York: Springer-Verlag, 1999.

[32] Y. Zhan and A. M. Knight, "Parallel time-stepped analysis of induction machines with Newton-Raphson iteration and domain decomposition," *IEEE Trans. Magn.*, vol. 44, no. 6, pp. 1546–1549, Jun. 2008.

[33] O.-R. Miron, D. Desideri, D. D. Micu, A. Maschio, A. Ceclan, and L. Czumbil, "Estimation of an equivalent short solenoid model using different numerical methods," *Arch. Elect. Eng.*, vol. 60, no. 4, pp. 433–444, 2011.

[34] K. Preis, O. Biro, M. Friedrich, A. Gottvald, and C. Magele, "Comparison of different optimization strategies in the design of electromagnetic devices," *IEEE Trans. Magn.*, vol. 27, no. 5, pp. 4154–4157, Sep. 1991.

[35] A. Kakaee and M. Kesshavarz, "Comparison the sensitivity analysis and conjugate gradient algorithms for optimization of opening and closing angles of valves to reduce fuel consumption in XU7/L3 engine," *Int. J. Autom. Eng.*, vol. 2, no. 3, 2012.

[36] A. Neculai, "Scaled memoryless BFGS preconditioned conjugate gradient algorithm for unconstrained optimization," *Optim. Meth. Softw.*, vol. 2, pp. 561–571, 2007.

[37] J. Trzasko and A. Manduca, "Highly undersampled magnetic resonance image reconstruction via homotopic l_0-minimization," *IEEE Trans. Med. Imag.*, vol. 28, no. 1, pp. 106–121, 2009.

[38] A. V. Knyazev, "Toward the optimal preconditioned eigensolver: Locally optimal block preconditioned conjugate gradient method," *SIAM J. Sci. Comput.*, vol. 23, no. 2, pp. 517–541, 2001.

[39] D. D. Micu, L. Czumbil, G. Christoforidis, and A. Ceclan, "Layer recurrent neural network solution for an electromagnetic interference problem," *IEEE Trans. Magn.*, vol. 47, no. 5, pp. 1410–1413, May 2011.

[40] Y. H. Dai and Y. Yuan, "An efficient hybrid conjugate gradient method for unconstrained optimization," *Ann. Oper. Res.*, no. 103, pp. 33–47, 2001.